

GT2011-46* &

Mu Analysis for Turbomachinery Stall Flutter

Md M.I. Forhad
 University of Central Florida
 Orlando, FL, USA

Puneet Vishwakarma
 University of Central Florida
 Orlando, FL, USA

Yunjun Xu
 University of Central Florida
 Orlando, FL, USA

ABSTRACT

Flutter is an aeroelastic instability phenomenon that can result either in serious damage or complete destruction of a gas turbine blade structure. To assure a reliable and safe operation, potential for blade flutter must be eliminated from the turbomachinery stages. In this paper, the robustness of an axial compressor blade design is studied with respect to parametric uncertainties through the Mu analysis. The analytical description of the nominal model used is based on matching a two dimensional incompressible flow field across the flexible rotor and the rigid stator. The aerodynamic load on the blade is derived via the control volume analysis. For use in the Mu analysis, first the model originally described by a set of partial differential equations is reduced to ordinary differential equations by the Fourier series based collocation method. After that, the nominal model is obtained by linearizing the achieved non-linear ordinary differential equations. The uncertainties coming from the modeling assumptions, model reduction, and linearization approximations, as well as imperfectly known parameters and coefficients are all modeled as parametric uncertainties through the Monte Carlo simulation. As compared with other robustness analysis tools, such as H_{inf} , the Mu analysis is less conservative and can handle both structured and unstructured perturbations. Simulation results show that the procedure described in this paper can be effective in studying the flutter stability margin and can be used to guide the gas turbine blade design.

Keywords: Flutter, gas turbine blade, Mu analysis, robustness

NOMENCLATURE

A_t : Throttle parameter
 B : Greitzer B parameter
 c : Rotor chord length
 c_s : Stator chord length
 D : Blade mass
 F_l : Lift force on the blade due to fluid flow
 I_{ea} : Moment of inertia of the blade about elastic axis
 \hat{i} : Unit vector in the axial direction

\hat{j} : Unit vector in the tangential direction
 L_c : Compressor duct length
 L_t : Inlet duct length
 L_r : Rotor pressure loss
 $L_{r,qs}$: Quasi-steady rotor total pressure loss
 $L_{s,qs}$: Quasi-steady stator total pressure loss
 L_{r1} : Coefficient of the empirical rotor loss function
 L_{r2} : Coefficient of the empirical rotor loss function
 L_{r3} : Coefficient of the empirical rotor loss function
 L_{s1} : Coefficient of the empirical stator loss function
 L_{s2} : Coefficient of the empirical stator loss function
 L_{s3} : Coefficient of the empirical stator loss function
 L_s : Stator pressure loss
 M : Aerodynamic moment about the elastic axis
 N_B : Number of blades
 p_{atm} : Atmospheric pressure non-dimensionalized by ρU_T^2
 Q_b : Frequency of the pure bending mode
 Q_t : Frequency of the pure torsion mode
 q : Bending displacement of the blade
 t : Non-dimensional time
 U_T : Tip Speed
 v : Non-dimensional tangential velocity, C_θ/U_T
 x : Axial coordinate
 X : States in the non-linear and linear models
 α : Torsional displacement of the blade
 β_r : Trailing edge metal angle of the rotor
 β_{zr} : Zero-incidence angle of the rotor leading edge
 β_{zs} : Zero-incidence angle of the stator leading edge
 γ_r : Stagger angle of the rotor
 γ_s : Stagger angle of the stator
 ε : Rotational inertia divided by chord
 Φ : Non-dimensional mass Flow, C_x/U_T

- $\tilde{\phi}$: Perturbation axial velocity
 - Ψ : Non-dimensional pressure, $P/\rho U_T^2$
 - Ψ_p : Non-dimensional plenum Pressure, $p_p/\rho U_T^2$
 - $\tilde{\psi}$: Perturbation pressure
 - τ_r : Time scale for the rotor loss
 - τ_s : Time scale for the stator loss
 - ξ_{ea} : Position of the elastic axis of the blade from the leading edge divided by the blade-chord
 - ξ_{cg} : Position of the center of gravity of the blade from the leading edge divided by the blade-chord
 - ξ_{cp} : Position of the center of pressure of the blade from the leading edge divided by the blade-chord
 - ζ_b : Structural damping of the bending mode
 - ζ_t : Structural damping of the torsion mode
 - δ_1 : Coefficient of the empirical rotor deviation function
 - δ_2 : Coefficient of the empirical rotor deviation function
- Subscripts:
- 1 : Inlet of the actuator disk
 - 2 : Exit of the rotor, inlet of the stator
 - 3 : Exit of the stator
 - le : Leading edge
 - rel : In the rotor (rotating) reference frame
 - r : Rotor
 - s : Stator
 - te : Trailing edge

INTRODUCTION

Gas turbines and other turbomachines constitute rotating blades and guiding vanes. As compared to vanes, blades are more susceptible to fluttering, and the risk of blade flutter in turbomachinery applications has received much attention due to the increasing operational demands and aggressive design requirements recently; for example high lift and low mass designs in aero-engines [1]. To assure a reliable jet propulsion, the potential for blade flutter must be eliminated from the turbomachinery stages [2].

Significant advances in the understanding of blade flutter have been achieved through numerous experimental and theoretical investigations. Much attention has been focused on compressors due to their well documented predisposition to blade flutter under certain operation regimes [1].

Although the advances in understanding the blade flutter have been quite significant, the current models for turbomachinery flutter are normally computationally intensive, and it is difficult to ensure high fidelity. Also, the number of states is prohibitively high such that a systematic analysis of the flutter phenomenon is not easy to achieve [2]. Reduced order models have been constructed to obtain a computationally more tractable system [3]. But these models suffer from either one or several of the following limitations: (1) not including the vibration mode shape, (2) modeling flows over a range of

geometries and Mach numbers may not be accomplished, (3) only valid for small amplitude oscillations about a large magnitude steady state.

Considering various shortcomings of the models resulting in lack of proper tools to predict flutter accurately, to ensure a safe operation it is therefore important to study the robustness of a turbomachinery blade design in the presence of uncertainties. In this paper the robustness of a compressor blade is studied with respect to parametric uncertainties.

FLUTTER MODEL

The compression system as shown in Fig. 1, composed of an inlet duct, an axial compressor stage of flexible rotors and rigid stators, a plenum chamber, and a throttle, is considered. The compressor pumps the flow into the plenum, which exhausts through a throttle. A high hub-to-tip ratio is assumed such that the flow can be treated as two-dimensional, with the variations considered in the axial and circumferential directions only. The compressor ducts are assumed to be long enough so that there is no non-axisymmetric pressure field interaction with the end terminations. The flow external to the blade rows is considered to be inviscid. Compressibility effects are neglected assuming low Mach numbers in the compressor and ducts. In the plenum, where the compressibility effects are important, density changes are related to the pressure changes through an isentropic relation [4]. Losses are introduced into the rotor and stator stages through the empirical total pressure loss relations. The flexible rotor blades are represented by a simple two dimensional, two degrees of freedom model, which is done using a typical section with an inertial and aerodynamic coupling between twist and plunge. A control volume analysis is used to couple the aerodynamics and structural dynamics, which provides the effect of the aeroelastic phenomenon. The deformed blade passages are defined and analyzed as a deformable control volume across flexible rotors coupled with a structural model [4-5].

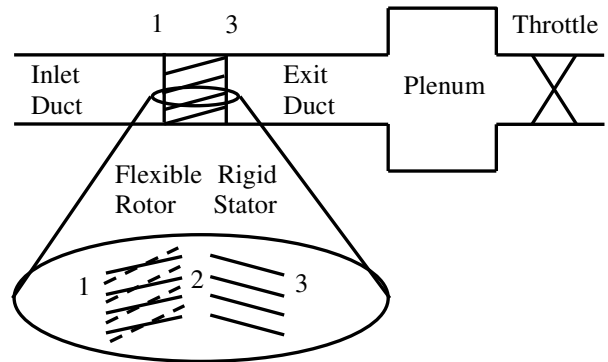


Fig. 1: Compression System Schematic

The equations of the flutter model used here are adopted from [4-5]. The equations have been reorganized in a form that can be easily used in the Mu analysis later. Detailed discussions on the model can be found in [4-10].

A- Inlet and Exit Duct

The annular inlet and exit ducts are assumed to have a constant height, and the flow is assumed to be incompressible.

In the inlet duct, only the potential flow perturbations can be created by the compressor and these decay upstream. Hence, for an axisymmetric meanflow, the linearized relation between the non-axisymmetric static pressure and the axial velocity perturbations at the inlet (station 1), as given in [7], is

$$\tilde{\psi}_1 = -\text{Re} \sum_{n=1}^N \left[\frac{1}{n} \frac{\partial \hat{\phi}_{1n}}{\partial t} + \bar{\phi}_1 \hat{\phi}_{1n}(t) \right] e^{in\theta} \quad (1)$$

where $\bar{\phi}_1 = (1/2\pi) \int_0^{2\pi} \Phi_1(t, \theta) d\theta$, and $\Phi_1 = \bar{\phi}_1 + \tilde{\phi}_1$. $\hat{\phi}_{1n}$ is the n^{th} harmonic component of non-axisymmetric axial velocity perturbation at station 1, while “Re” denotes the real part of the complex term in Eq. (1) and N is the highest number of harmonics used to describe the inlet axial velocity Φ_1 .

In the exit duct, the only disturbances considered are the decaying potential field downstream and the vorticity associated with the variation in the compressor loading around the annulus. The analysis is simplified by the assumption that the stators fix the exit flow angle to be axial (i.e. no deviation effects). This produces the following relation between the non-axisymmetric pressure distribution at the exit of the compressor (Station 3) and the flow perturbations [7].

$$\tilde{\psi}_3 = \text{Re} \sum_{n=1}^N \left[\frac{1}{n} \frac{\partial \hat{\phi}_{3n}}{\partial t} \right] e^{in\theta} \quad (2)$$

$\hat{\phi}_{3n}$ is the n^{th} harmonic component of non-axisymmetric axial velocity perturbation at station 3. Equations (1) and (2) are used together with Equations (32) and (36), which are shown later in this paper, to calculate the pressures at stations 1 and 3.

B- Plenum and Throttle

As shown in [4], the conservation of the axial momentum in the inlet and exit ducts, and the conservation of the mass in an isentropic plenum results in the following equations:

$$\frac{1}{2\pi} \int_0^{2\pi} \left[(\Psi_3 - \Psi_1) - \Psi_p = L_c \frac{\partial \Phi_1}{\partial t} \right] d\theta \quad (3)$$

and

$$\frac{1}{2\pi} \int_0^{2\pi} \left[\Phi_1 - A_r \sqrt{2\Psi_p} = 4B^2 L_c \frac{\partial \Psi_p}{\partial t} \right] d\theta \quad (4)$$

Equations (3) and (4) are related to two states: Φ_1 and Ψ_p .

C- Blade Dynamics

As described by Dowel [11] and Gysling and Myers [6], the structural dynamics of the blade is modeled considering a typical section with the inertial and aerodynamic coupling between the twist and plunge motions. The lift force is assumed to act at the center of pressure, which is assumed constant. The

two modes considered here are the twist and plunge as illustrated in Fig. 2.

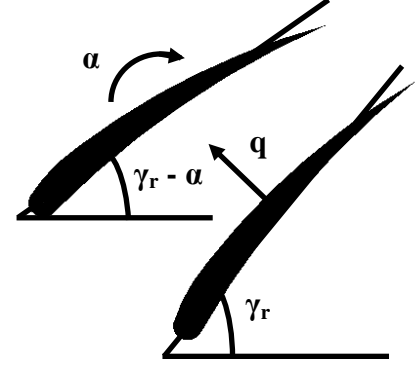


Fig. 2: Blade deflection indicating the positive sense of twist α and plunge q (modified based on [5])

The plunge equation is described by

$$\begin{aligned} & \left(\frac{\partial}{\partial t} - \frac{\partial}{\partial \theta} \right)^2 q + (\xi_{ea} - \xi_{cp}) c \left(\frac{\partial}{\partial t} - \frac{\partial}{\partial \theta} \right)^2 \alpha \\ & + 2\zeta_b Q_b \left(\frac{\partial}{\partial t} - \frac{\partial}{\partial \theta} \right) q + Q_b^2 q = \frac{F_l}{D} \end{aligned} \quad (5)$$

while the twist equation is

$$\begin{aligned} & \left(\frac{\partial}{\partial t} - \frac{\partial}{\partial \theta} \right)^2 \alpha + \frac{(\xi_{ea} - \xi_{cg}) c D}{I_{ea}} \left(\frac{\partial}{\partial t} - \frac{\partial}{\partial \theta} \right)^2 q \\ & + 2\zeta_t Q_t \left(\frac{\partial}{\partial t} - \frac{\partial}{\partial \theta} \right) \alpha + Q_t^2 \alpha = \frac{M}{I_{ea}} \end{aligned} \quad (6)$$

where the moment of inertia I_{ea} can be calculated by

$$I_{ea} = D (\xi_{ea} - \xi_{cg})^2 c^2 + D c^2 \varepsilon^2 \quad (7)$$

The lift force on the blade F_l in Eq. (5) is calculated by

$$F_l = \frac{F_\theta \cos(\gamma_r - \alpha) - F_x \sin(\gamma_r - \alpha)}{2} \quad (8)$$

where F_x and F_θ are axial and circumferential components of the force on the blade $\vec{F} = F_x \hat{i} + F_\theta \hat{j}$. F_x and F_θ can be calculated through the control volume analysis across two adjacent blades to be describe in the next section. The moment about the elastic axis in Eq. (6) is given by

$$M = F_l (\xi_{ea} - \xi_{cp}) c \quad (9)$$

There are four state variables in Equations (5) and (6): α , $\dot{\alpha}$, q and \dot{q} .

D- Control Volume Analysis

The two components of the force on the blade, F_x and F_θ , can be calculated based on the conservation of the momentum equation across the rotor described by

$$\begin{aligned} & \left(\frac{\partial}{\partial t} - \frac{\partial}{\partial \theta} \right) \left(\bar{v} \frac{\partial V}{\partial \theta} \right) + [\bar{v}_{te} (\bar{v}_{rel,te} \cdot \bar{n}_{te}) + p_{te} \bar{n}_{te}] \frac{\partial s_{te}}{\partial \theta} \\ & + [\bar{v}_{te} (\bar{v}_{rel,te} \cdot \bar{n}_{te}) + p_{te} \bar{n}_{te}] \frac{\partial s_{te}}{\partial \theta} = - \frac{\partial \vec{F}}{\partial \theta} \end{aligned} \quad (10)$$

where

$$\frac{\partial V}{\partial \theta} = c \cos(\gamma_r - \alpha) \frac{1}{2} \left(\frac{\partial s_{le}}{\partial \theta} + \frac{\partial s_{te}}{\partial \theta} \right) \quad (11)$$

Force exerted on the blade by the fluid is found by

$$\vec{F} = \int_{\theta_b - \pi/N_B}^{\theta_b + \pi/N_B} [\partial \vec{F} / \partial \theta] d\theta \quad (12)$$

where θ_b is the blade angular position, which is constant for a blade with respect to a fixed reference.

The two path lengths along the leading and trailing edges can be calculated by

$$\frac{\partial s_{le}}{\partial \theta} = \sqrt{\left(\frac{\partial x_{le}}{\partial \theta} \right)^2 + \left(\frac{\partial \theta_{le}}{\partial \theta} \right)^2} \quad (13)$$

and

$$\frac{\partial s_{te}}{\partial \theta} = \sqrt{\left(\frac{\partial x_{te}}{\partial \theta} \right)^2 + \left(\frac{\partial \theta_{te}}{\partial \theta} \right)^2} \quad (14)$$

respectively. The axial and circumferential coordinates of the leading and trailing edges are given by

$$x_{le} = -q \sin(\gamma_r) - \xi_{ca} c \cos(\gamma_r - \alpha) \quad (15)$$

$$\theta_{le} = \theta + q \cos(\gamma_r) - \xi_{ca} c \sin(\gamma_r - \alpha) \quad (16)$$

$$x_{te} = -q \sin(\gamma_r) + (1 - \xi_{ca}) c \cos(\gamma_r - \alpha) \quad (17)$$

$$\theta_{te} = \theta + q \cos(\gamma_r) + (1 - \xi_{ca}) c \sin(\gamma_r - \alpha) \quad (18)$$

The two normal vectors at the blade leading and trailing edges used in Eq. (10) are found as

$$\vec{n}_{le} = -\cos(\beta_{le}) \hat{i} + \sin(\beta_{le}) \hat{j} \quad (19)$$

$$\vec{n}_{te} = \cos(\beta_{te}) \hat{i} - \sin(\beta_{te}) \hat{j} \quad (20)$$

The relative velocities between the flow and the two edges of the blade used in Eq. (10), $\vec{v}_{rel,le}$ and $\vec{v}_{rel,te}$, are given by

$$\vec{v}_{rel,le} = (\Phi_1 \hat{i} + v_1 \hat{j}) - \left(\frac{\partial}{\partial t} - \frac{\partial}{\partial \theta} \right) (x_{le} \hat{i} + \theta_{le} \hat{j}) \quad (21)$$

and

$$\vec{v}_{rel,te} = (\Phi_2 \hat{i} + v_2 \hat{j}) - \left(\frac{\partial}{\partial t} - \frac{\partial}{\partial \theta} \right) (x_{te} \hat{i} + \theta_{te} \hat{j}) \quad (22)$$

The axial component of the velocity at the rotor leading edge (station 1) Φ_1 is found from Eq. (3) while the circumferential component v_1 is calculated by the following assumption as suggested by Moore and Greitzer [8]

$$\frac{\partial v_1}{\partial \theta} = -\tilde{\phi}_1 \quad (23)$$

The axial and circumferential velocities at the trailing edge of the rotor (station 2), Φ_2 and v_2 , can be found from the conservation of mass equation together with an assumption on flow kinematics. The conservation of mass equation is expressed as

$$\left(\frac{\partial}{\partial t} - \frac{\partial}{\partial \theta} \right) \frac{\partial V}{\partial \theta} + (\vec{v}_{rel,le} \cdot \vec{n}_{le}) \frac{\partial s_{le}}{\partial \theta} + (\vec{v}_{rel,te} \cdot \vec{n}_{te}) \frac{\partial s_{te}}{\partial \theta} = 0 \quad (24)$$

The kinematic constraint on the flow is based on the assumption that the fluid exits the blade with a certain deviation

angle described by an empirical relation. Following is the equation of kinematic constraint on the flow.

$$v_2 - \left(\frac{\partial}{\partial t} - \frac{\partial}{\partial \theta} \right) \theta_{te} = \left[\Phi_2 - \left(\frac{\partial}{\partial t} - \frac{\partial}{\partial \theta} \right) x_{te} \right] \tan(\beta_r - \alpha + \delta) \quad (25)$$

where the flow deviation angle at the exit of the rotor, δ , is assumed to be a function of the incidence angle given by

$$\delta = \delta_1 \alpha_{inc,r} + \delta_2 \quad (26)$$

The rotor incidence angle $\alpha_{inc,r}$ is given by

$$\alpha_{inc,r} = \tan^{-1} \left(\frac{\vec{v}_{rel,le} \cdot \hat{j}}{\vec{v}_{rel,le} \cdot \hat{i}} \right) - \beta_{cr} + \alpha \quad (27)$$

The velocity within the control volume, \vec{v} in Eq. (10), is approximated by the average of the leading and trailing edge flow velocities as

$$\vec{v} = \frac{1}{2} (\vec{v}_{le} + \vec{v}_{te}) \quad (28)$$

where

$$\vec{v}_{le} = \Phi_1 \hat{i} + (1 + v_1) \hat{j} \quad (29)$$

$$\vec{v}_{te} = \Phi_2 \hat{i} + (1 + v_2) \hat{j} \quad (30)$$

The axisymmetric pressure at the leading edge $\bar{\Psi}_1$ can be calculated by the unsteady Bernoulli's equation [12]

$$p_{am} - \bar{\Psi}_1 = \frac{1}{2} (\Phi_1^2 + v_1^2) + L_r \frac{\partial \Phi_1}{\partial t} \quad (31)$$

Thus the expression for p_{le} in Eq. (10), which is essentially the pressure at station 1 Ψ_1 , is given by

$$p_{le} = \Psi_1 = \bar{\Psi}_1 + \tilde{\psi}_r = p_{am} - \frac{1}{2} (\Phi_1^2 + v_1^2) + \tilde{\psi}_r \quad (32)$$

The trailing edge pressure p_{te} used in Eq. (10) can be calculated from the conservation of energy, when the force term in the equation is substituted by the LHS of the conservation of momentum equation. The conservation of energy across the deforming blade passage is given by

$$\left(\frac{\partial}{\partial t} - \frac{\partial}{\partial \theta} \right) \frac{1}{2} v^2 \frac{\partial V}{\partial \theta} + \left(p_{le} + \frac{1}{2} v_{le}^2 - L_r \right) (\vec{v}_{rel,le} \cdot \vec{n}_{le}) \frac{\partial s_{le}}{\partial \theta} + \left(p_{te} + \frac{1}{2} v_{te}^2 \right) (\vec{v}_{rel,te} \cdot \vec{n}_{te}) \frac{\partial s_{te}}{\partial \theta} = - \frac{\partial \vec{F}}{\partial \theta} \cdot \vec{v}_{cv} \quad (33)$$

where L_r represents a loss in the leading edge total pressure to account for non-conservative processes, which is governed by Eq. (37) shown in the next section. The velocity of the control volume is approximated by the average of the velocities of the leading and trailing edge boundaries.

$$\vec{v}_{cv} = \left(\frac{\partial}{\partial t} - \frac{\partial}{\partial \theta} \right) \left(\frac{x_{le} + x_{te}}{2} \hat{i} + \frac{\theta_{le} + \theta_{te}}{2} \hat{j} \right) + \hat{j} \quad (34)$$

E- Analysis for the Stator

The stator is modeled as a rigid blade row, and the conservation of mass across the stator can be expressed as

$$\Phi_2 = \Phi_3 \quad (35)$$

Using the unsteady Bernoulli's equation [4], the following relation is found to govern the pressure rise across the stator

$$(\Psi_{t,3} - \Psi_{t,2}) = \frac{c_s}{\cos(\gamma_s)} \frac{\partial \Phi_2}{\partial \tau} - L_s \quad (36)$$

where L_s represents a loss in the total pressure across the stator, which is governed by Eq. (38) to be shown in the next section. $\Psi_{2,t}$ is the total pressure at the trailing edge of the rotor, while $\Psi_{3,t}$ is the total pressure at the trailing edge of the stator.

F- Rotor and Stator Losses

The total pressure losses across the rotor and stator disks are assumed to lag their quasi-static values. A simple one dimensional lag equation is used in each case [5].

$$\tau_r \left(\frac{\partial}{\partial t} - \frac{\partial}{\partial \theta} \right) L_r = -(L_r - L_{r,qs}) \quad (37)$$

$$\tau_s \left(\frac{\partial}{\partial t} - \frac{\partial}{\partial \theta} \right) L_s = -(L_s - L_{s,qs}) \quad (38)$$

The quasi-static losses $L_{r,qs}$ and $L_{s,qs}$ are assumed to be functions of incidence angle,

$$L_{r,qs} = L_{r1} \alpha_{inc,r}^2 + L_{r2} \alpha_{inc,r} + L_{r3} \quad (39)$$

$$L_{s,qs} = L_{s1} \alpha_{inc,s}^2 + L_{s2} \alpha_{inc,s} + L_{s3} \quad (40)$$

The incidence angle on the rotor is defined in Eq. (27). The incidence angle on the stator is given by

$$\alpha_{inc,s} = -\tan^{-1} \left(\frac{v_2}{\phi_2} \right) - \beta_{zs} \quad (41)$$

Equations (37) and (38) result in two states in the model: L_r and L_s .

REDUCED ORDER MODEL via THE FOURIER SERIES BASED COLLOCATION METHOD

To be used in the stability and robustness analysis, the PDE model described in the above section is reduced to an ODE form through the Fourier series based collocation approach following the steps described in [13].

The state variables Φ_1 , α , q , L_r and L_s in the model are approximated in terms of the Fourier series as shown below.

$$\Phi_1 = \sum_{n=0}^N [\hat{\varphi}_n(t) \cos(n\theta) + \hat{\phi}_n(t) \sin(n\theta)] \quad (42)$$

$$\alpha = \sum_{n=0}^N [a_n(t) \cos(n\theta) + \hat{a}_n(t) \sin(n\theta)] \quad (43)$$

$$q = \sum_{n=0}^N [b_n(t) \cos(n\theta) + \hat{b}_n(t) \sin(n\theta)] \quad (44)$$

$$L_r = \sum_{n=0}^N [lr_n(t) \cos(n\theta) + \hat{lr}_n(t) \sin(n\theta)] \quad (45)$$

$$L_s = \sum_{n=0}^N [ls_n(t) \cos(n\theta) + \hat{ls}_n(t) \sin(n\theta)] \quad (46)$$

in which N is the highest number of harmonics used in the series.

Plenum pressure Ψ_p is assumed to be spatially uniform and hence approximated by a time dependent term only.

$$\Psi_p = \psi_0(t) \quad (47)$$

The unknown variables in the original PDEs are then substituted by the approximation and the residual functions are obtained at the collocation points. In this paper, the two boundary points of integration and their midpoint are used as the collocation points. A set of ODEs is then obtained by forcing the residual functions to be zero at the collocation points. For brevity, Eq. (37), the rotor loss equation, is used as an example to demonstrate the basic procedure.

$$\tau_r \left(\frac{\partial}{\partial t} - \frac{\partial}{\partial \theta} \right) L_r = -(L_r - L_{r,qs}) \quad (48)$$

If $N = 1$, the unknown variable rotor loss L_r is approximated by

$$L_r = lr_0(t) + lr_1(t) \cos(\theta) + \hat{lr}_1(t) \sin(\theta) \quad (49)$$

Now substituting L_r in Eq. (48) by the approximation in Eq. (49), following residual equation can be obtained at $\theta = \theta_i$, where $i = 1, 2, 3$.

$$\tau_r \left(\frac{dlr_0(t)}{dt} + \frac{dlr_1(t)}{dt} \cos \theta + \frac{d\hat{lr}_1(t)}{dt} \sin \theta + lr_1(t) \sin \theta - \hat{lr}_1(t) \cos \theta \right) = -(lr_0(t) + lr_1(t) \cos \theta + \hat{lr}_1(t) \sin \theta - L_{r,qs}) \quad (50)$$

The residual equation can be reorganized to obtain a state space representation.

Comparing the simulations with different number of harmonics in the Fourier series approximation, it is found that a series approximation with only zeroth and first order harmonic is sufficient to capture the system dynamics. Following are the 22 states in the reduced order non-linear model:

Variables	States
Φ_1	$\Phi_0, \Phi_1, \hat{\Phi}_1$
Ψ_p	ψ_0
α	$a_0, a_1, \hat{a}_1, \dot{a}_0, \dot{a}_1, \hat{\dot{a}}_1$
q	$b_0, b_1, \hat{b}_1, \dot{b}_0, \dot{b}_1, \hat{\dot{b}}_1$
L_r	lr_0, lr_1, \hat{lr}_1
L_s	ls_0, ls_1, \hat{ls}_1

The nonlinear model of the whole compression system in terms of the 22 state variables are then organized in the form of
$$\begin{bmatrix} \dot{X} \end{bmatrix}_{22 \times 1} = [A]_{22 \times 22} [X]_{22 \times 1} + [B]_{22 \times 22} [\sqrt{X}]_{22 \times 1} + [f(X, p)]_{22 \times 1} \quad (51)$$
 where $f(X, p)$ is a function of the states, X , and parameter vector p . Matrices $[A]$ and $[B]$ are found to be constant for each operating point; $[A][X]$ denotes the linear part of the model. For the model achieved here, matrix $[B]$ has only one non-zero entry, as the governing equation of the plenum pressure is the only equation in the model with a square root term. Non-linearity of the system comes mainly from the part $f(X, p)$.

LINEARIZED MODEL and STABILITY ANALYSIS

First the equilibrium point of the system (Eq. 51) is found for a throttle parameter (A_s) setting. Then the non-linear model is linearized about the equilibrium point X_{eq} by means of the small perturbation theory. First the partial derivatives of $f(X, p)$ with respect to all the state variables X are found numerically, by using a five point stencil formula. All the partial derivatives of $[B][\sqrt{X}]$ can be found analytically. Finally, the Taylor series expansion is utilized to obtain the linearized function for the original non-linear function. All the three matrices combined together, the linearized perturbation model is obtained in the form of
$$\begin{bmatrix} \Delta \dot{X} \end{bmatrix}_{22 \times 1} = [Z]_{22 \times 22} [\Delta X]_{22 \times 1},$$
 where $X = X_{eq} + \Delta X$.

The eigenvalues of the linear model are calculated to study the stability of the system. All the eigenvalues of the system are shown in Fig. 3. A representative eigenvalue of the system as found in each iteration of the Monte Carlo simulation (explained in next section) is presented in Fig. 4.

From Fig. 3 and Fig. 4, it can be seen that all the eigenvalues of the system are in left half of the complex plane, which indicates a stable system for the uncertainty bounds used.

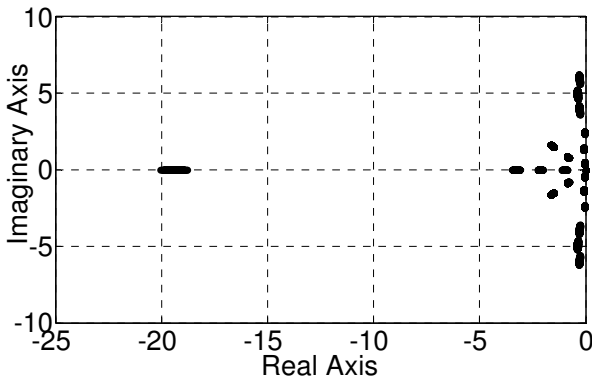


Fig. 3: Eigenvalues of the system (all eigenvalues shown together)

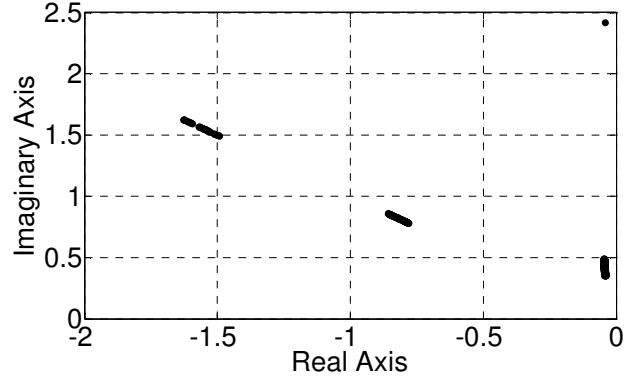


Fig. 4: A representative eigenvalue of the system (for all iterations of Monte Carlo simulations)

QUANTIFICATION of UNCERTAINTY BOUNDS via MONTE CARLO SIMULATION

Because of a number of assumptions and simplifications, which have been made at different levels, the nominal model may not be an exact representation of the system. Secondly, the model reduction approximations also cause uncertainties in the model. Thirdly, the linearization causes uncertainties to the model due both to truncation of the Taylor series and the calculation of partial derivatives numerically. Furthermore, the parameters and coefficients used in the obtained nominal model are not perfectly known.

To find the uncertainty bounds on the nominal model, the Monte Carlo simulation is done for the system with some bounded random variation of some of the parameters. The mean model obtained from Monte Carlo simulations is used as the nominal model for the Mu Analysis.

The parametric uncertainties considered here are mainly on some of the structural properties which might vary slightly from the design value because of the manufacturing and installation processes. For example all the blades are not exactly the same. Different blades might have slightly different frequencies for bending and twist modes, and different damping ratios. Also a small uncertainty is considered in some of the geometry parameters, which may be caused by wear and tear etc.

Following are the structural properties in which uncertainties are considered with their nominal values:

Structural damping of bending mode, $\zeta_b = 0.035$

Frequency of pure bending mode, $Q_b = 1.5$

Structural damping of torsion mode, $\zeta_t = 0.035$

Frequency of pure torsion mode, $Q_t = 3.3$

The geometry parameters considered to have uncertainties and their nominal values are:

Position of the elastic axis of the blade from leading edge divided by blade-chord, $\xi_{ea} = 0.55$

Position of the center of gravity of the blade from leading edge divided by blade-chord, $\xi_{cg} = 0.35$

Position of the center of pressure of the blade from leading edge divided by blade-chord, $\xi_{cp} = 0.35$

The following empirical coefficients are also considered to have uncertainties:

Time scale for rotor loss, $\tau_r = 0.61$

Time scale for stator loss, $\tau_s = 0.32$

Coefficient of empirical rotor deviation function, $\delta_1 = 0.18$

Coefficient of empirical rotor deviation function, $\delta_2 = 12^\circ$

Coefficient of empirical rotor loss function, $L_{r1} = 1.8842$

Coefficient of empirical rotor loss function, $L_{r2} = -0.5053$

Coefficient of empirical rotor loss function, $L_{r3} = 0.1219$

Coefficient of empirical stator loss function, $L_{s1} = 0.7429$

Coefficient of empirical stator loss function, $L_{s2} = -0.1450$

Coefficient of empirical stator loss function, $L_{s3} = 0.0951$

For obtaining a number of linear models and uncertainty bounds on the model, three different percentages of uncertainties are assumed on structural parameters-- 1%, 2.5% and 5% respectively. For all the cases considered in this paper, the empirical coefficients are assumed to have 5% uncertainty about their nominal values while considering the state of the art manufacturing processes that most often can obtain any geometry very accurately, the geometry parameters in the model are considered to have only 1% uncertainty.

In the Monte Carlo simulations, each of the parameter is defined with a random variation about the nominal value within the uncertainty ranges described above. The linear model is obtained in each iteration of the Monte Carlo simulation. A total of 1,000 iterations are used in the simulations to quantify the uncertainty bounds on the nominal model.

MU SYNTHESIS

In this section, the basic steps, in using the Mu analysis tool [19-25] to analyze the robust performance of the system in presence of parametric uncertainties in the system, are shown.

The linearized system obtained in the previous section can be written as:

$$\begin{aligned} \dot{X} &= [A]_{22 \times 22} X + [B]_{22 \times 22} u \\ y &= [I]_{22 \times 22} X \end{aligned} \quad (52)$$

where B is a zero matrix because the system under analysis is open loop. The system output is the state. All the uncertainties in matrix A are modeled as additive parametric uncertainties as $A = (\hat{A} + W\Delta)$, where \hat{A} is the mean value obtained in the Monte Carlo simulation, and $W = [W]_{22 \times 22}$ contains the uncertainty boundary magnitude for each of the entries in matrix A . Δ is any kind of uncertainties with a magnitude upper bounded by 1.

The following are the basic steps involved in obtaining the synthesis model for the Mu analysis with the uncertainties accounted. The magnitudes of the uncertainty, their position in

the main equation and their numbers are unique which vary with each equation. Let us use the first state equation as an example to show the basic approach.

$$\dot{X}_1 = \sum_{j=1}^{22} (A_{1,j} + W_{1,j}\Delta) X_j \quad (53)$$

Rewriting Eq. (53), the following equation is obtained.

$$\dot{X}_1 = \sum_{j=1}^{22} (A_{1,j} X_j + W_{1,j} X_j \Delta) \quad (54)$$

Let's define $W_{1,j} X_j \triangleq z_j$; Eq. (54) can then be written as:

$$\dot{X}_1 \triangleq \sum_{j=1}^{22} (A_{1,j} X_j + z_j \Delta) \quad (55)$$

Eq. (55) can be further written as

$$\dot{X}_1 \triangleq \sum_{j=1}^{22} A_{1,j} X_j + w_j \quad (56)$$

with the definition $z_j \Delta \triangleq w_j$.

Similarly, equations for the remaining 21 states are derived. For a particular throttle parameter value, the input and output relations derived for the open loop model is shown in Fig. 5. In this model, there are 207 uncertainty signals input to the open loop P from the uncertainty block Δ as shown in Fig. 6. In the meantime, there are 207 signals $z_i, i = 1, \dots, 207$ coming into the uncertainty block Δ from the open loop model P .

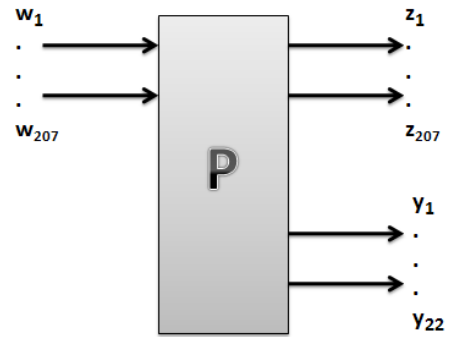


Fig. 5: Open-loop model with the input/output relations

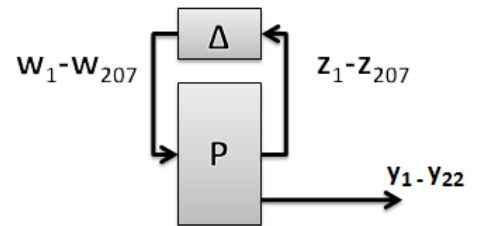


Fig. 6: Synthesis model

The synthesized model is written in state space form as shown in Eq. (57) including states $[X] \in \mathbb{R}^{22 \times 1}$, exogenous signals $[w, u] \in \mathbb{R}^{229 \times 1}$, uncertainty input signals $z \in \mathbb{R}^{207 \times 1}$ and output signals $y \in \mathbb{R}^{22 \times 1}$

$$P = \begin{bmatrix} A_{22 \times 22} & B_{22 \times 229} \\ C_{229 \times 22} & D_{229 \times 229} \end{bmatrix} \quad (57)$$

ROBUST STABILITY ANALYSIS

The structured singular value μ from the Robust Control Toolbox in MATLAB[®] is used to analyze the robustness of the uncertain flutter model based on the synthesis model in Fig. 6. As discussed in the previous section, for the particular throttle setting, the outputs of the synthesis system are composed of the output of the system and input to the uncertainty block. For calculating the robust performance, the frequency response of the system is calculated with the real uncertainty block specified. In this section the results of this analysis are discussed.

Three different cases with throttle parameter $A_t = 0.7$ are presented first here. Case I is a system with small uncertainty of 1% on all the parameters. As can be seen in the μ plot in Fig. 7, the system is robustly stable to modeled uncertainty because the μ value is less than one for all frequencies. Case II is a system with an uncertainty of 2.5% in the parameter values. From Fig. 8 it can be seen that this uncertain system is not robustly stable to the modeled uncertainty for certain frequencies. It can tolerate up to 30.9% of the modeled uncertainty and a destabilizing combination of 114% of the modeled uncertainty exists causing instability at 2.15 rad/s. Case III involves a system with a relatively higher uncertainty of 5% on the structural parameters. It is shown in Fig. 9 that the design is not robust with respect to the defined uncertainty. A destabilizing combination of 89.5% of the modeled uncertainty exists causing an instability at 2.73 rad/s. In addition to the stability conclusions obtained from the three cases we can get useful information about the frequency range the systems are stable within and the frequency that corresponds to the peak value of μ .

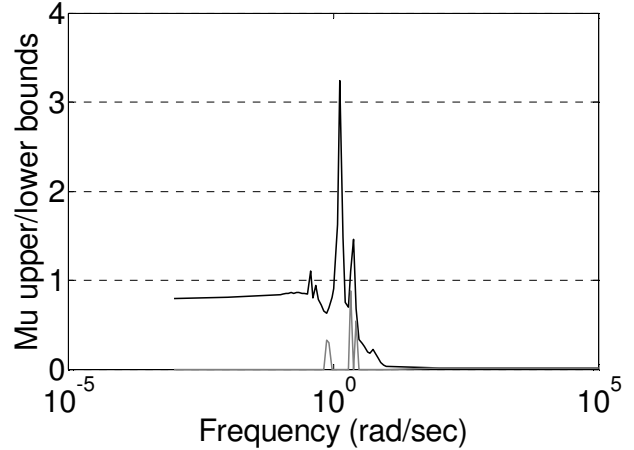


Fig. 8: Robust Analysis of Case II Flutter Model

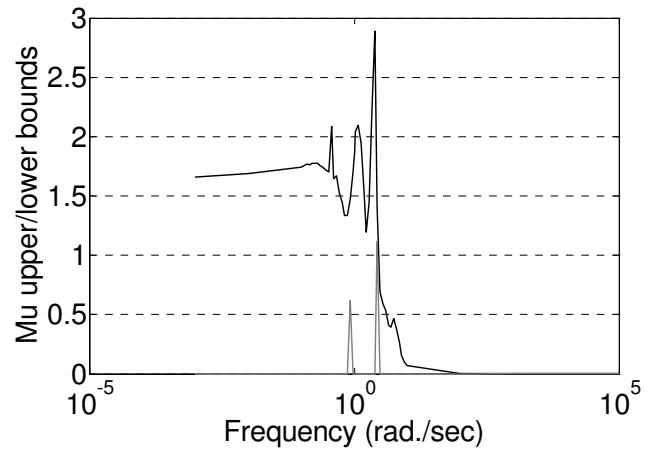


Fig. 9: Robust Analysis of Case III Flutter Model

μ analysis is then done on the system with 5% uncertainties on the structural parameters at two new operating points. The μ plots for Case IV represented by throttle parameter $A_t = 0.6$, and Case V represented by $A_t = 0.9$ are shown in Fig. 10 and Fig. 11 respectively.

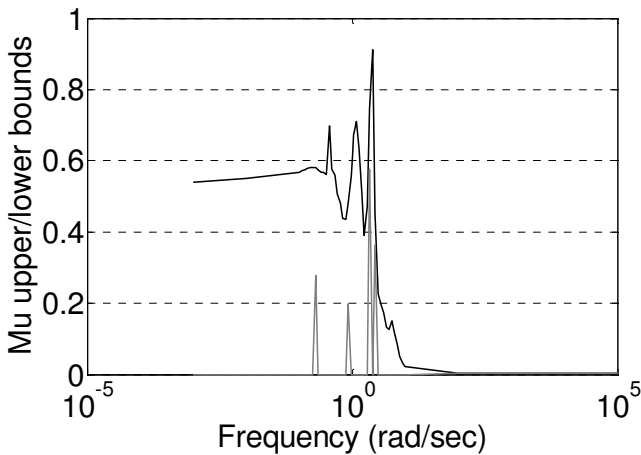


Fig. 7: Robust Analysis of Case I Flutter Model

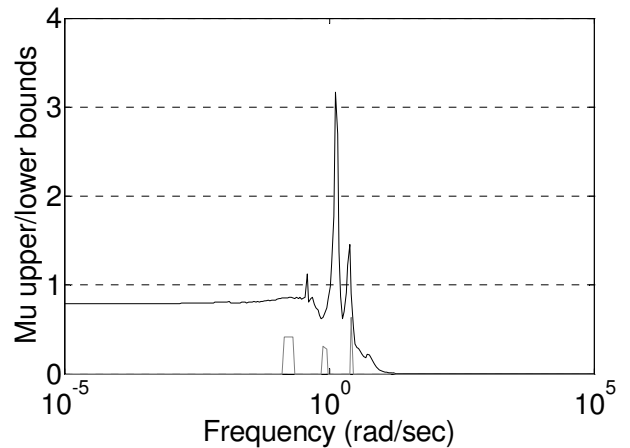


Fig. 10: Robust Analysis of Case IV Flutter Model

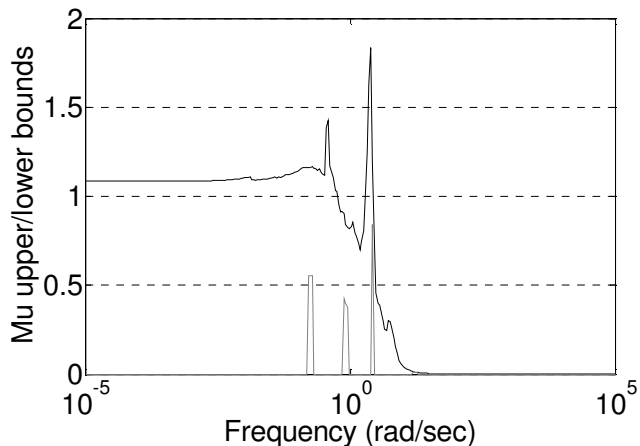


Fig. 11: Robust Analysis of Case V Flutter Model

Looking at the Mu plot for Cases III, IV and Case V, which all have 5% uncertainty on structural parameters but different operating points, it is found that the frequency corresponding to the maximum value of Mu does not shift much depending on operating point. Hence a new set of values are assigned to the structural parameters to see if the frequency corresponding to the peak value of Mu would shift based on nominal values of the parameters. New values assigned for the structural properties are shown below:

Structural damping of bending mode, $\zeta_b = 0.025$

Frequency of pure bending mode, $Q_b = 2.75$

Structural damping of torsion mode, $\zeta_t = 0.025$

Frequency of pure torsion mode, $Q_t = 5.5$

The Mu plot for the new values of parameters with 5% uncertainty on structural parameters is shown in Fig. 12.

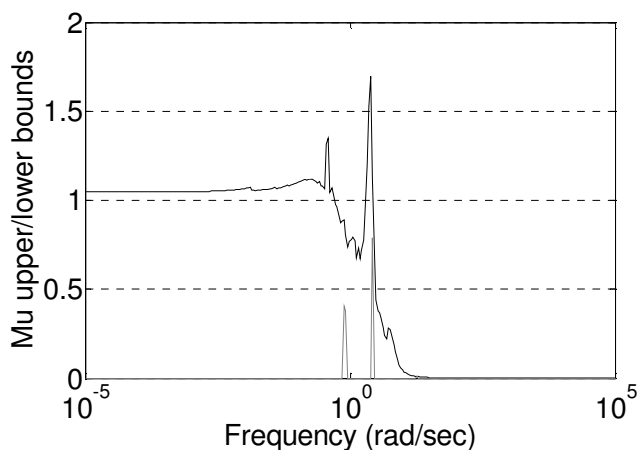


Fig. 12: Robust Analysis of Case VI Flutter Model

As seen in Fig. 12, like the previously stated cases with 5% uncertainties on the structural parameters, the system is not robustly stable for the modeled uncertainty. The peak frequency occurs at 2.42 rad/sec, which does not indicate a shift in frequency corresponding to instability based on changes in nominal value of structural parameters. Hence the authors investigated the linear models obtained for both cases and found that out of the 22 natural frequencies of the linear system, mainly the highest frequency is affected by the change in nominal values of structural parameters while the lower frequencies are not affected significantly. As a result the frequency corresponding to the peak value of Mu does not shift depending on nominal value of parameters, since it is the lower frequencies that are easily excited. Table- 1 shows some higher and lower natural frequencies of the linear model obtained in Cases III and VI using different nominal values of structural parameters.

Natural Frequency	Case III Model	Case VI Model
High Frequencies (rad/sec)	16.8	22.5
	5.93	5.94
	4.94	4.96
Low Frequencies (rad/sec)	2.42	2.42
	2.21	2.21
	1.16	1.16

Table – 1: Natural frequencies of linear models III and VI

CONCLUSION

In this paper, the Mu tool is applied to analyze the robustness of a gas turbine compressor blade in terms of flutter. In this analysis, uncertainties, such as the ones arising from unmodeled dynamics, model order reduction, linearization, and imperfectly known parameters, are all considered. The nominal model and uncertainty bounds used in the Mu analysis are obtained via the Monte Carlo simulation based on a linearized model reduced from a publicly available two dimensional, incompressible flow model coupled with structural dynamics.

To do an accurate robust performance analysis using Mu tool, a model that can capture the physical phenomenon approximately is necessary. Mu tool can give very accurate result, when the robustness analysis with respect to parametric uncertainties is done based on an accurate model. In case of absence of an accurate model, the uncertainty bound on the nominal model would be high and a design using Mu tool could be too conservative. With a high accuracy model and the steps shown in this paper, the robust performance of the compressor blades can be determined accurately and used by designers to predict safe operation conditions such that unstable operation regions can be avoided.

ACKNOWLEDGMENTS

This work was funded by the Florida Center for Advanced Aero-Propulsion (FCAAP). The support is gratefully acknowledged.

REFERENCES

- [1] Rice, T., Bell, D., Singh, G., "Identification of the Stability Margin between Safe Operation and the Onset of Blade Flutter," *Proceedings of ASME Turbo Expo 2007: Power for Land, Sea and Air*, Montreal, Canada, May 14-17, 2007.
- [2] Khalak, A., "A Framework For Flutter Clearance of Aeroengine Blades," *Proceedings of ASME TURBO EXPO 2001*, New Orleans, Louisiana, June 4-7, 2001.
- [3] Epureanu, B.I., "A parametric analysis of reduced order models of viscous flows in turbomachinery," *Journal of Fluids and Structures*, 17, 2003, pp 971-982.
- [4] Wong, M.T.M., "System Modeling and Control Studies of Flutter in Turbomachinery", MS Thesis, Massachusetts Institute of Technology, 1997.
- [5] Copeland, G.S., and Rey, G., "Non-linear Modeling, Analysis and Control of Turbomachinery Stall Flutter," *Air Force Office of Scientific Research Contract Report*, AFRL-SR-BL-TR-98-0694, 1998.
- [6] Gysling, D.L. and Myers, M.R., "A framework for analyzing the dynamics of Flexibly-Bladed Turbomachines," *ASME 96-GT-440, Intl Gas Turbine and Aeroengine Congress and Exhibition*, Birmingham, U.K., June 10-13, 1996
- [7] Longley, J.P., "A Review of Nonsteady Flow Models for Compressor Stability," *Journal of Turbomachinery*, Vol. 116, April 1994, pp. 202-215.
- [8] Moore, F.K., Greitzer, E.M., "A Theory of Post Stall Transients in Axial Compression Systems: Part I and II," *ASME Journal of Engineering for Gas Turbine and Power*, Vol. 108, 1986, pp 68-76.
- [9] Adamczyk, J. J. et al, "Supersonic Stall Flutter of High Speed fans," *Journal of Engineering for Power*, Vol. 104, 1982, pp. 675-682.
- [10] Adamczyk, J. J., "Analysis of Supersonic Stall Bending Flutter in Axial Flow Compressor by Actuator Disk Theory," *NASA technical Paper 1345*, Nov 1978.
- [11] Dowell, et al. *A Modern Course in Aeroelasticity*, Sijthoff and Noordhoff, Alphen aan den Rijn, The Netherlands, 1978.
- [12] Zaeit, C., Akhrif, O., Saydy, L., "Modeling and Non-linear Control of a Gas Turbine," *Proceedings of IEEE International Symposium on Industrial Electronics*, Montreal, Quebec, Canada, July 9-12, 2006.
- [13] Boyd, J.P., *Chebyshev and Fourier Spectral Methods*, New York, Dover Publications Inc., 2000.
- [14] Bell, D.L., and He, L., "Three Dimensional Unsteady Flow for an Oscillating Turbine Blade and the Influence of Tip Leakage," *ASME Journal of Turbomachinery*, Vol. 122, No. 1, 2000, pp 93-101.
- [15] Bölcs, A., Fransson, T.H., "Aeroelasticity in Turbomachine: Comparison of Theoretical and Experimental Cascade Results," *Communication du Laboratoire de Thermique Thermique Appliquée et de Turbomachines*, 1986, No. 13, Lusuanne, EPFL.
- [16] Boyce, P. M., *Gas Turbine Engineering Handbook*, 3rd Ed., Burlington MA, Elsevier Inc., 2006, pp. 310-311.
- [17] Carta, F.O, and St. Hilaire, A.O., "Effects of Interblade Phase Angle on Cascade Pitching Stability," *ASME Journal of Engineering for Power*, Vol. 102, 1980, pp. 391-396
- [18] Whitehead, D. S., "Vibration of Cascade Blades Treated by Actuator Disk Methods," *Proceedings of the Institute of Mechanical Engineers*, Vol. 173, no. 21, pp. 555-574.
- [19] Balas, G. J., Doyle, J. C., Glover, K., Packard, A., and Smith, R., *μ -Analysis and Synthesis Toolbox: User's Guide*. The Mathworks Inc., 1991.
- [20] Balas, G., Chiang, R., Packard, A., and Sofonov, M., *Robust Control Toolbox: User's Guide*. Natick, MA: MathWorks, 2005.
- [21] Hoekstra, D., "QFT robust control design and MU analysis for a solar orbital transfer vehicle," The Netherlands, Technische Universiteit Eindhoven, 2004.
- [22] Lind, R., and Brenner, M., "Flutterometer: An On-Line Tool to Predict Robust Flutter Margins," *Journal of Aircraft*, Vol. 37, No. 6, 2000, pp. 1105-1112.
- [23] Micklow, J and Jeffers, J., "Semi-Actuator Disk Theory for Compressor Choke Flutter," *NASA Contract Report NAS3-20060*, Oct 1980
- [24] Xu, Y., Fitz-Coy, N., Lind, R., and Tatsch, A., " μ Control for Satellites Formation Flying," *Journal of Aerospace Engineering*, Vol. 20, 2007, pp. 10-21.
- [25] Xu, Y., Suman, S., "Robust Stationkeeping Control for Libration Point Quasi-Periodic Orbits," *Journal of Aerospace Engineering*, Vol. 21, No. 2, April 1, 2008, pp. 102-115.